Journal of The Electrochemical Society, **153** (3) A595-A606 (2006)
0013-4651/2006/153(3)/A595/12/$20.00 © The Electrochemical Society

Characterization of the Lithium Surface in *N*-Methyl-*N*-alkylpyrrolidinium Bis(trifluoromethanesulfonyl)amide Room-Temperature Ionic Liquid Electrolytes

P. C. Howlett,[a] N. Brack,[b] A. F. Hollenkamp,[c] M. Forsyth,[a,*] and D. R. MacFarlane[d]

[a]*Department of Materials Engineering, Monash University, ARC Centre for Nanostructured Electromaterials, Clayton, Victoria 3800, Australia*
[b]*Centre for Materials and Surface Science, Department of Physics, La Trobe University, Victoria, Bundoora, Victoria 3083, Australia*
[c]*CSIRO, Energy Technology, Clayton South, Victoria 3169, Australia*
[d]*School of Chemistry, Monash University, Clayton, Victoria 3800, Australia*

The solid electrolyte interphase (SEI) formed on a lithium electrode in an *N*-methyl-*N*-alkylpyrrolidinium bis(trifluoromethanesulfonyl)amide [$p_{1,x}(Tf)_2N$] room-temperature ionic liquid electrolyte was characterized using X-ray photoelectron spectroscopy, diffuse reflectance Fourier transform infrared spectroscopy, Raman spectroscopy, and electrochemical impedance spectroscopy (EIS). The SEI was found to be composed mainly of reduction products of the $(Tf)_2N^-$ anion. A pronounced difference in composition was observed between the SEI formed on the lithium surface and that formed in situ during lithium deposition on a copper substrate. In the case of the lithium surface, native surface species (e.g., Li_2O, Li_2CO_3) persisted in the SEI and dominated the SEI composition. The surface film formed on lithium-deposited-on-copper did not contain species associated with the lithium native film. Instead, in addition to the anion reduction products, significant quantities of species associated with the cation were observed. EIS indicated varied lithium conduction pathways through the film and that the pathways were in series, suggesting a layered structure. Calculated activation energies, resistivity, and thickness values were comparable to literature values for the SEI formed in conventional liquid electrolytes.
 [DOI: 10.1149/1.2164726]

Manuscript submitted August 9, 2005; revised manuscript received November 29, 2005. Available electronically February 1, 2006.

The use of a lithium metal electrode in conjunction with a room-temperature ionic liquid (RTIL) electrolyte offers a potential solution to the safety concerns and poor cycle-life that have prevented the development of safe rechargeable lithium metal batteries. These batteries offer significant improvements, in terms of the specific capacity of the negative electrode, over present lithium-ion technology. RTILs are attractive for use as electrolytes in rechargeable lithium batteries because of their electrochemical stability, high conductivity, thermal stability, low safety hazard (nonvolatile and nonflammable), and low toxicity. Particularly, the inert properties of RTILs are attractive because of the potential to provide safer operation, allow high-temperature cycling, and allow scale-up to large devices.

Lithium metal electrodes have not been successfully implemented in secondary cells because of problems that arise when lithium undergoes repetitive deposition and dissolution (corresponding to charge and discharge cycling of a cell). Invariably, cycling of the lithium metal electrode results in a dendritic morphology, which presents safety problems and results in a drastically shortened cycle life.[1] It is widely accepted that the solid electrolyte interphase (SEI) is mainly responsible for the electrochemical behavior of lithium metal.[2,3] Considerable efforts have been expended to characterize the lithium surface in organic electrolytes, and to gain an understanding of how this is reflected in the lithium electrochemistry. It has been established that a native film covers the surface of commercially available lithium foil. The film consists of various compounds—LiOH, Li_2O, Li_3N, (Li_2O-CO_2) adduct or Li_2CO_3. These compounds are produced by the reaction of lithium with O_2, H_2O, CO_2, or N_2.[4,5] After contact with aprotic organic electrolytes, reduction products of the electrolyte components (including impurities) cover the lithium surface. Typically, alkyl carbonates reduce to lithium alkyl carbonates ($ROCO_2Li$), esters reduce to alkoxy species (ROLi) and alkyl carboxylate species (RCOOLi). In addition, inorganic reduction products of the electrolyte salt and impurities such as water were found to be present (e.g., LiF, Li_2O, and LiOH).

Recently, we have reported that the RTIL, *N*-methyl-*N*-alkylpyrrolidinium bis(trifluoromethanesulfonyl)amide [$p_{1,X}(Tf)_2N$, shown below in I and II], can be used as a solvent for lithium electrochemistry and that high lithium cycling efficiency can be obtained.[6] The presence of an SEI formed from reduction products of the $(Tf)_2N^-$ anion was proposed and X-ray photoelectron spectroscopy (XPS) data presented as evidence

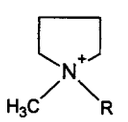

(I) $p_{1,X}^+$ R = propyl, butyl.

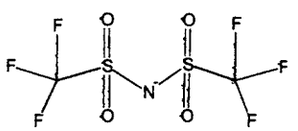

(II) $(Tf)_2N^-$

Papers that report lithium electrochemistry in RTILs often refer to the formation of a passivating film to explain the observed behavior.[7-10] Recently numerous reports have appeared in the literature detailing studies of RTILs as electrolytes in lithium ion cells, where film forming additives have been used to prevent intercalation of the RTIL cation at the anode.[11-16] In addition, reports of RTIL lithium metal cells have appeared, occasionally with additives or as polymer gels.[17-22] The majority of these studies utilize either an imidazolium or quaternary ammonium cation with a $(Tf)_2N^-$ anion. Several authors have reported that the addition of $Li(Tf)_2N$ extends the cathodic limit of the system.[6,10,23] All of this implies a role for the $(Tf)_2N^-$ anion in providing additional stability to such systems for lithium electrochemistry. Indeed, evidence suggesting the formation of a protective film on the lithium surface in a $Li(Tf)_2N/p_{1,4}(Tf)_2N$ electrolyte has been reported by other workers.[24] However, to our knowledge, the composition and structure of the SEI formed in a RTIL electrolyte has not been the subject of a publication. Here, we present the details of XPS measurements

* Electrochemical Society Active Member.

as well as supporting Fourier transform infrared spectroscopy diffuse reflectance (DRFTIR), in situ Raman microscopy, and electrochemical impedance spectroscopy (EIS) data. The information is used to expand the description of the SEI formed in $p_{1,X}(Tf)_2N$ electrolytes as presented in our earlier publication.[6]

Experimental

Electrolyte preparation.— The $p_{1,3}(Tf)_2N$ and $p_{1,4}(Tf)_2N$ RTILs used in this study were prepared in our laboratories according to MacFarlane et al.[25] Following synthesis, the RTILs were characterized by IR spectroscopy, ^1H and ^{13}C NMR spectroscopy, and electrospray mass spectroscopy. Thermal properties and purity were also determined by DSC and TGA. The neat RTILs were dried in a vacuum oven at 90°C for over 24 h. The liquid was then degassed overnight with a stream of dried argon to remove additional water and dissolved gases. Electrolytes were prepared by adding the required amount of the dried lithium salt of the anion [e.g., $Li(Tf)_2N$ to $p_{1,3}(Tf)_2N$] to give a concentration (molality) in mol (lithium salt) per kg (solution). The salt was allowed to dissolve at 50°C overnight.

Sample preparation.— Surface analysis was performed on lithium and lithium-deposited-on-copper electrodes (denoted Li and Li-Cu, respectively) removed from cycled Li/0.5 mol kg^{-1} $Li(Tf)_2N$-$p_{1,X}(Tf)_2N$/Cu cells. The cells were cycled galvanostatically using a deposition and dissolution current density of 0.25 mA cm^{-2}. Initially, 1 C cm^{-2} of lithium was deposited on the copper electrode and then 0.25 C cm^{-2} of lithium was cycled for 10 deposition-dissolution cycles. Because of the non-volatile nature of the RTIL, it was not possible to remove it from the surface of the sample by evaporation prior to characterisation. Any solvent capable of removing the RTIL from the surface was also likely to compromise the sample. Instead, the bulk of the RTIL was removed by physical means (mounted on an electric motor and spun at high speed under argon). Thus, all of the measurements were conducted with the RTIL persisting on the sample surface.

X-ray photoelectron spectroscopy.— The sample was mounted on an XPS sample stud using conductive carbon adhesive tape and placed in an hermetic transference vessel for transfer to the instrument. The samples were admitted to the XPS instrument without exposure to the atmosphere by enclosing the sample introduction chamber in an argon filled glove bag. Spectra were acquired on a Kratos Axis Ultra imaging XPS spectrometer. An aluminum monochromated X-ray source operating at 10 mA and 15 kV (150 W) was focused on the sample surface. The hybrid analysis mode was used which provided a sampling area of 300 × 700 μm. Survey spectra were acquired at 160 eV pass energy and high resolution region spectra were acquired at 20 eV pass energy. The instrument vacuum was maintained at $\sim 1.2 \times 10^{-8}$ Torr. Etching experiments were performed on the sample surface using an argon ion beam gun operating at 15 mA and 5 kV, resulting in an estimated etching rate of ~ 1 Å s^{-1}. Instrument operation and peak fitting was performed using the XPS Axis ultra software. A 70:30 Gaussian:Lorentzian algorithm was used to fit the peaks to obtain quantitative results. The fit produced an estimated ±10% error in the atomic concentration determined for each peak.

Diffuse reflectance Fourier-transform infrared spectroscopy.— Infrared spectra were acquired on a Digilab FTS 3000MX Excalibur series spectrometer using Digilab Win-IR Pro 3.2 software. Ex situ diffuse reflectance (DRFTIR) spectra were obtained using a Harrick DRFTIR accessory. To protect the sample surface from reaction with the atmosphere a hermetic transference chamber was designed and built, in which the DRFTIR accessory was housed. The chamber incorporated KBr O-ring sealed windows and an O-ring sealed access door. The chamber was aligned such that the windows and DRFTIR accessory could be positioned in the instrument beam path. Transmission spectra for the electrolyte were obtained using NaCl windows.

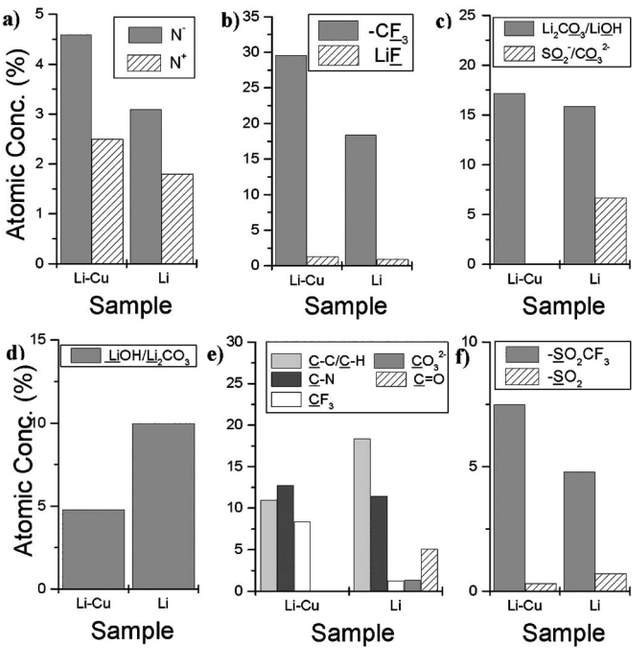

Figure 1. Atomic concentration (%) summary determined from the region spectra for the Li and Li-Cu surface (estimated error ±10%): (a) N 1s region, (b) F 1s region, (c) O 1s region, (d) Li 1s region, (e) C 1s region, (f) S 2p region.

Raman microscopy.— Raman spectra were acquired on a Renishaw RM2000 Raman spectrograph. The spectrograph was equipped with a HeNe 632.8 nm Spectraphysics laser source. In situ and ex situ spectra were acquired using an Olympus BH2 microscope attachment with 5×, 20×, and 50× objective lenses. The system was controlled by a PC operating Renishaw WiRE (Windows Renishaw Environment) software V1.3. In situ spectra were acquired from an optical cell fitted with a borosilicate window, as described in an earlier publication.[26] Ex situ spectra were acquired from samples that were housed within a specially designed cell incorporating a borosilicate window that could be sealed in the glove box.

Electrochemical impedance spectroscopy.— Impedance spectroscopy was performed using a Solartron DI 1296 dielectric interface and a Solartron S1 1270 frequency response analyzer under GPIB control from a PC using Solartron Impedance Measurement software. A Eurotherm 2204e temperature controller under serial control was used to control a 240V cartridge heater and a K-type thermocouple mounted in a brass block which heated the samples. Each impedance spectrum was acquired using a 5 mV ac perturbation versus the cell open-circuit voltage (OCV). The ac perturbation was varied from 10^7 to 0.05 Hz for each temperature. Measurements were typically made from 25 to 80°C in 10°C steps (the first step being 5°C) on heating. A second spectrum was acquired at 10°C intervals from 80 to 30°C on cooling. Impedance spectra were fitted to equivalent circuits using ZView version 2.3 (Scribner Associates 1999-2000).

Results and Discussion

X-ray photoelectron spectroscopy (XPS).— XPS high-resolution region spectra peak identities were determined from published stan-

dard values[27] and from reports from XPS studies of the lithium surface.[28-35] Initial measurements clearly indicated that the RTIL was present on the surface of the sample in significant quantities, as expected after sample preparation. This is testament to the lack of volatility of these electrolyte materials, given that the results indicate that the RTIL is present, apparently unchanged, under ultrahigh vacuum ($\sim 10^{-8}$ Torr).

Figure 1 presents a graphical summary of the results obtained from typical high-resolution region spectra comparing the lithium (Li) and lithium-deposited-on-copper surface (Li-Cu). The bulk electrolyte contained a Li^+:$p^+_{1,X}$:$(Tf)_2N^-$ molar ratio of approximately 1:4:5. Thus, by determining a mass balance for each of the species present, it was possible to account for the RTIL that persisted on the surface and gain an indication of which species were present in excess (or deficit). The departure from the "electrolyte ratio" most likely reflects the composition of the surface film, either in terms of new species present on the surface (excess), or in terms of the species that have been consumed to form the film (deficit). Generally, it was found that there were excess components of $(Tf)_2N^-$, lithium (as salts) and in the case of the lithium surface, excess oxygen, fluoride and carbonate species. With respect to the $p^+_{1,X}$ cation there was generally a small excess of C-N species and a slight deficit for C-C/C-H, this was more pronounced on the Li-Cu surface than it was on the Li surface. The $(Tf)_2N^-$ anion exhibited an excess in the amount of CF_3 and a deficit in the amount of SO_2 on the Li-Cu surface and a large excess of O (present as Li_2O) and a deficit of SO_2 on the Li surface.

Overall, the initial scans indicated that the surface was largely composed of lithium salts (covered by persistent RTIL), the majority of which appeared to be reduction products of the $(Tf)_2N^-$ anion. In addition, the results indicated a clear difference between the Li and Li-Cu surfaces. Carbonate and carbonyl species were present on the Li surface and absent on the Li-Cu surface; presumably, these were components of the native film. The Li-Cu surface also contained a larger fraction of $(Tf)_2N^-$ products than the Li surface, possibly due to the absence of the native film components. The Li surface contained a higher ratio of Li^+ (as salt) than the Li-Cu surface, indicating that the components of the film were associated with small and/or multivalent anions, i.e., a greater proportion of components such as Li_2O,Li_2CO_3 and LiF.

XPS etching experiments.— The data obtained from the previous experiments are only indicative of the outer surface of the sample. Photoelectrons are statistically only likely to be ejected from the outer few atomic layers of the sample (tens of angstroms), thus much of the SEI structure was not accessed. However, by bombarding the sample surface with sputtered argon ions, it is possible to etch the surface, thereby revealing the material underneath.

The etching process is a destructive technique and, as such, the process can alter the sample composition. Thus, the identification of changes in chemical states with depth needs to be considered carefully.[27] Therefore, conclusions drawn about the structure of the SEI from the etching experiments can only be tentative and must be supported by evidence from other techniques. Nevertheless, the etching process may still reveal new species likely to at least be present in the SEI, providing important insight into the nature of the film. The etching rate is estimated at roughly 1 Å s^{-1}, thus the etching experiments are estimated to have removed approximately 200-300 nm of material, which approximates the total thickness of the film (as estimated from EIS measurements later).

High-resolution region spectra were acquired initially, after 15 min and after 30 min for the Li sample and after 41 min for the Li-Cu sample. The results obtained from the high-resolution region spectra for both samples are summarized in Fig. 2 and 3.

Considering the F 1s spectra first (Fig. 2), peaks were identified for $-CF_3$ at 689.0 eV and LiF at 685.5 eV. The amount of $-CF_3$ present in the sample decreased significantly with etching, presumably due to the removal of the RTIL, and there was an increase in the quantity of LiF. The results suggest that a layer of LiF was present close to the lithium surface. There was also a significant difference between the samples, the Li surface quickly becoming dominated by LiF whereas the Li-Cu sample exhibited a more steady change, suggesting that the Li-Cu SEI may be thicker, or that a significant quantity of another species may be present on the Li surface, displacing the LiF.

Peaks present in the O 1s high-resolution region spectrum were identified as CO_3^{2-} or SO_2^- at 532.5 eV, Li_2CO_3 or LiOH at 532.0 eV, and Li_2O at 528.5 eV (Fig. 2). The results clearly indicate that the amount of CO_3^{2-} and SO_2 (predominately SO_2, referring to the S 2p and C 1s spectra) decreased and that the quantity of Li_2O was increasing. The Li sample showed a much larger quantity of Li_2O present on the surface. Li_2CO_3 or LiOH (not distinguishable) was also present, the Li surface containing a more significant quantity than the Li-Cu surface.

The N 1s high-resolution region spectrum displayed peaks corresponding to N^+ at 402.0 eV and N^- at 399.0 eV (Fig. 2). The results were consistent with the removal of the RTIL along with the surface during etching. Again, the concentration on the Li surface changed more quickly suggesting a thinner surface dominated by more reduced species. The Li surface also contained a small quantity of nitride species (at 397.5 eV), possibly related to the native film.

The C 1s high-resolution region spectrum indicated the presence of species associated with C-C/C-H at 285.0 eV, C-N at 286.5 eV, $-CF_3$ at 293.0 eV, CO_3^{2-} at 290.0 eV, and a species with C=O character, possibly an ester, at 288.0 eV (Fig. 3). There was a marked difference between the two surfaces, the Li surface showing steady removal of the carbons associated with the RTIL and the appearance of carbonate/carbonyl species. The Li-Cu surface displayed an increase for carbon, derived either from the cation or from the anion, although it seems most likely to be related to the organic cation. The other species, CF_3 and the carbonate/carbonyls showed similar distribution to those found for the Li surface.

The results obtained for the S 2p high-resolution region spectrum indicate the presence of $-SO_2CF_3$ species at 169.0 and 170.2 eV (doublet), oxidized sulfur species (sulfone, sulfite) at 167.0 and 168.2 eV (doublet) and a number of peaks most likely associated with elemental sulfur and sulfide species (presumably lithium sulfide) from 160-165 eV (Fig. 3). The $-SO_2CF_3$ moiety dissipated rapidly with etching, the high initial value probably consisted of reduced $(Tf)_2N^-$, as well as contributions from the RTIL persisting on the surface. At longer etching times, both samples displayed a complex mixture of reduced sulfur species, which adhered to the fitting parameters surprisingly well (i.e., a S 2p species produces a doublet arising from spin orbit splitting, the doublet should be separated by 1.18 eV and have a ratio of $\sim$2:1).[27] The overall quantity of sulfur species remained the same, becoming progressively more reduced, which is suggestive of changes due to the etching process. However, this could also reflect a progressively more reducing environment, close to the lithium surface. A small amount of oxidized sulfur ($-SO_2$) was present throughout the experiment.

The Li 1s high-resolution region spectrum displayed peaks corresponding to Li° at 52.5 eV, Li_2O at 54.0 eV, Li_2CO_3/LiOH at 55.3 eV, and LiF at 56.0 (Fig. 3). The initial Li surface spectrum indicated the presence of a significant quantity of Li_2CO_3/LiOH that did not persist with etching, and was possibly present as a contaminant arising from sample exposure to the glove box atmosphere. A large quantity of Li_2O is indicated for the Li surface, as well as a substantial amount of LiF, the quantity of Li_2O continued to increase with etching. The Li-Cu surface exhibited a single peak associated with LiF, which quickly reached a maximum concentration and stabilized in a similar manner to the Li surface.

A clear difference is evident between the native lithium surface and the surface of electrochemically deposited lithium. If the etching process is assumed to result in gradual removal of material and hence progressively uncovered surface species closer to the lithium surface, then a picture of the structure of the SEI

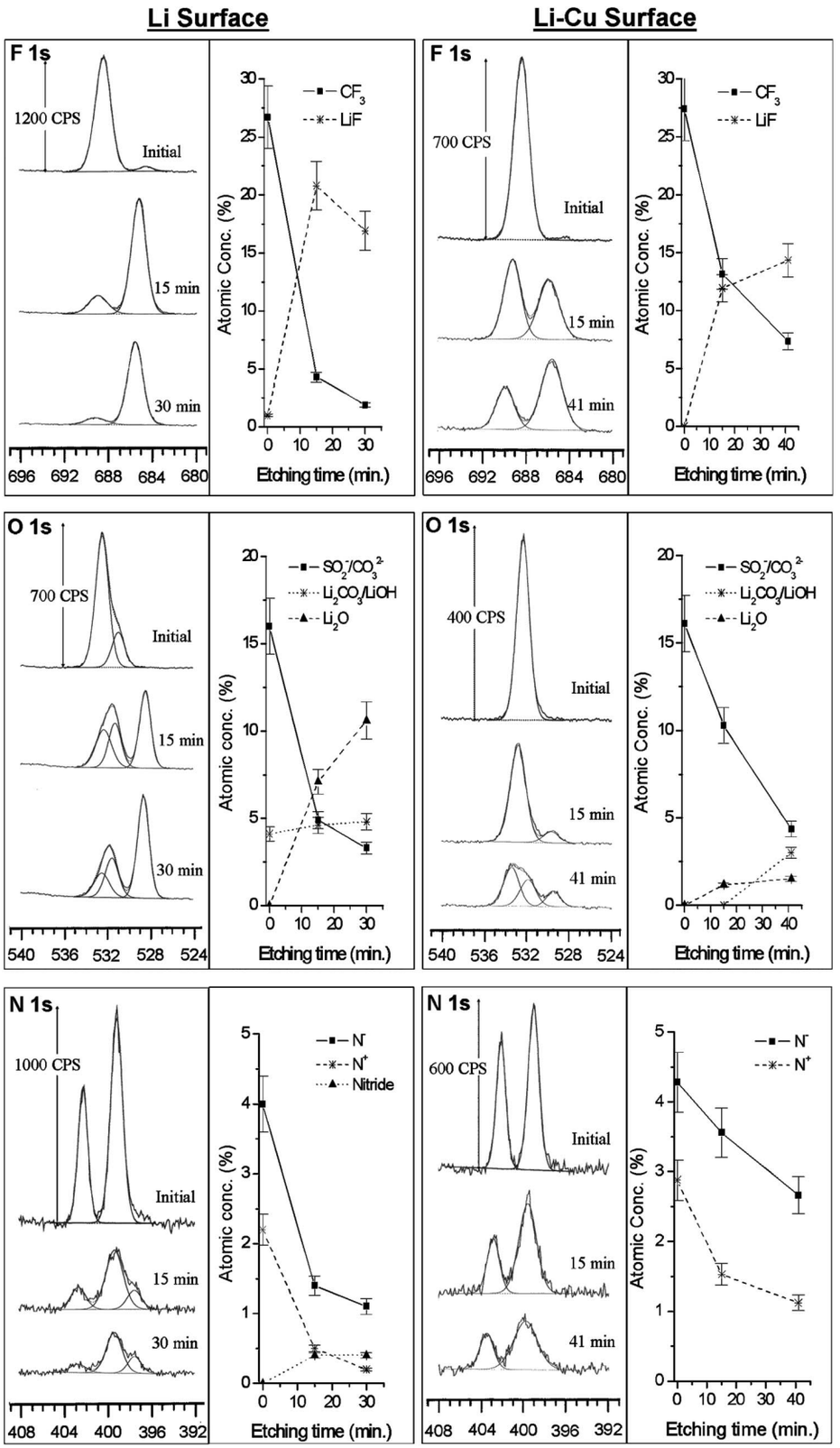

Figure 2. High-resolution F 1s, O 1s, and N 1s photoelectron spectra for the Li and Li-Cu surfaces before and after etching.

can be developed. The SEI formed on lithium metal was composedof an outer layer of less reduced $(Tf)_2N^-$ reduction products, e.g., $Li_2S_2O_4$, $Li_2NSO_2CF_3$, $Li_yC_2F_x$, etc. as well as Li_2O, LiOH, Li_2CO_3, and LiF. Etching indicated that, further in, LiF and Li_2O dominate the SEI, ultimately Li_2O appears to become the dominant species.. Products of this type have been proposed by Aurbach

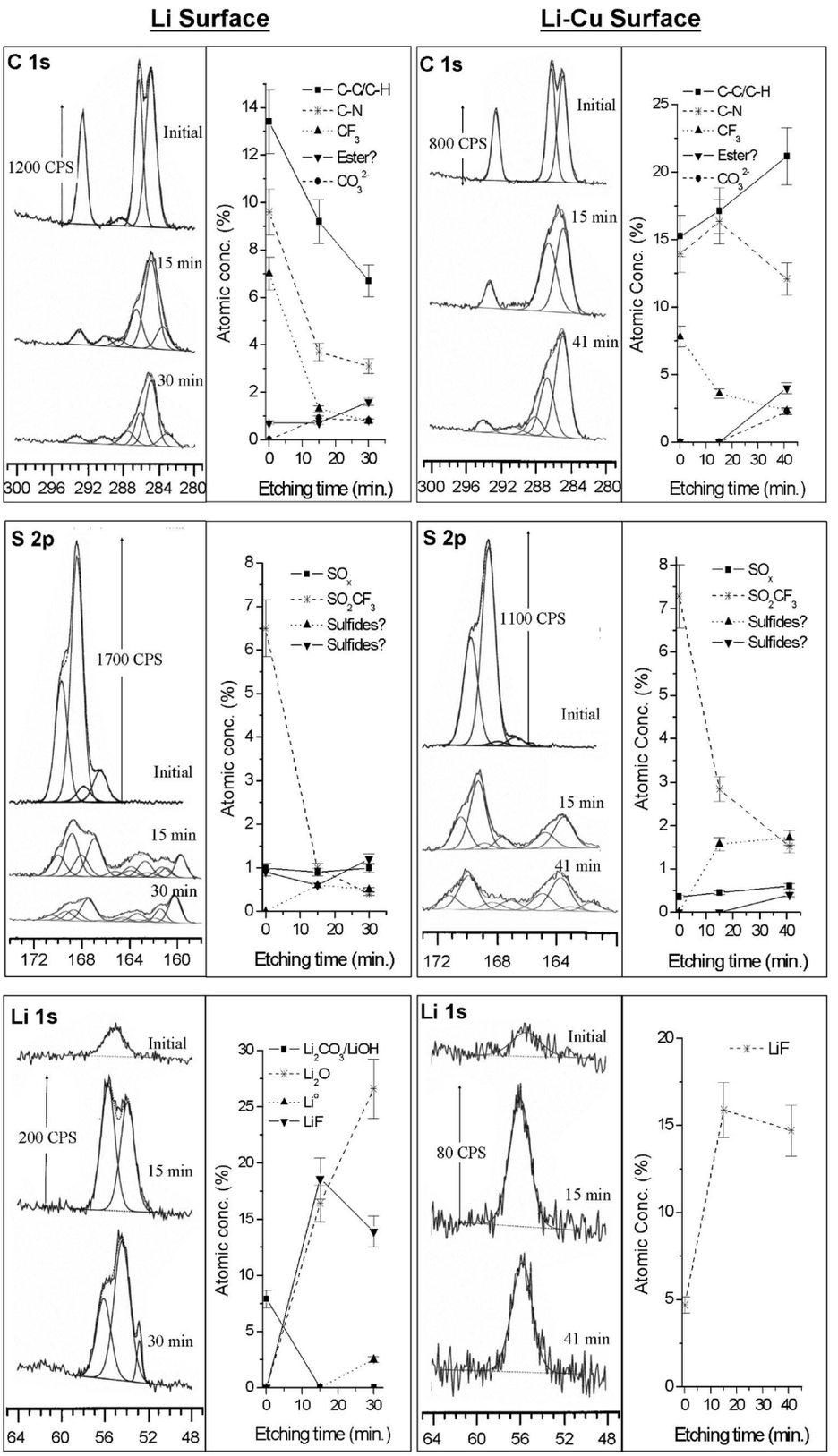

Figure 3. High-resolution C 1s, S 2p, and Li 1s photoelectron spectra for the Li and Li-Cu surfaces before and after etching.

et al.[36,55] as reduction products of $Li(Tf)_2N$ containing electrolytes. Aurbach's proposed reaction scheme involves the following partly sequential process

$$LiN(SO_2CF_3)_2 + ne^- + nLi^+ \rightarrow Li_3N + Li_2S_2O_4 + LiF + C_2F_xLi_y \quad [1]$$

Table I. Peak position and assignments for Raman and FTIR spectra of $p_{1,X}(Tf)_2N$ electrolytes.

Assignment	Raman	IR (cm^{-1})	Reference(s)
	314 (m)		
ρSO_2	327 (m)		37
	339 (m)		
ωSO_2	404 (m)		37
	437 (w)		
	496 (w)		
$\delta_a CF_3$		514 (m)	37
νN-C,$\delta_s SO_2$	553 (m)		38
νN-C,$\delta_a CF_3$	571 (w)	574 (m)	38
	590 (w)		
$\delta_a SO_2$		618 (s)	37
	636 (w)		
δSNS	657 (w)	655 (m)	37
	678 (w)		
$\delta_s CF_3$	743 (vs)	740 (m)	37, 39, and 40
ν_sSNS		762 (w)	37 and 40
νCS	798 (w)	790 (m)	37
	823 (w)		
Ring mode	889 (sh)	887 (w)	38 and 41
Ring mode	903 (m)	905 (w)	41
Ring mode		939 (w)	38 and 41
Ring mode		970 (w)	41
	1011 (w)	1004 (w)	
ν_aSNS	1041 (m)	1057 (s)	37
$\nu_s SO_2$	1138 (m)	1139 (s)	37
		1193 (s)	
$\nu_a CF_3$		1234 (sh)	37
τCH_2,$\nu_s CF_3$	1243 (s)		38
$\nu_{a}SO_{2(o.p.)}$	1332 (m)	1335 (sh)	37 and 40
$\nu_{a}SO_{2(i.p.)}$	1354 (m)	1354 (s)	37 and 40
δCH_2	1457 (m)	1434 (w)	38 and 41
νCH_2,νCH_3		1470 (m)	
δCH_2 (ring)	1493 (w)		38
νCH_2	2850 (w)		42
νCH_2	2889 (m)	2890 (m)	41
νCH_2		2949 (m)	42
νCH_2	2976 (s)	2981 (s)	41
νCH_2	2997 (s)		41
		3041 (w)	

$$LiN(SO_2CF_3)_2 + 2e^- + 2Li^+ \rightarrow Li_2NSO_2CF_3 + CF_3SO_2Li \quad [2]$$

$$Li_2S_2O_4 + 6e^- + 6Li^+ \rightarrow 2Li_2S + 4Li_2O \quad [3]$$

$$Li_2S_2O_4 + 4e^- + 4Li^+ \rightarrow Li_2SO_3 + Li_2S + Li_2O \quad [4]$$

Although the two situations [i.e., IL vs $Li(Tf)_2N$ in conventional solvents] are significantly different, particularly in terms of concentration, it is not surprising to find similar species on the lithium surface in a $(Tf)_2N^-$ based IL. Aurbach's work plainly indicates that the $(Tf)_2N^-$ anion is reactive under these conditions.

The deposited lithium surface (Li-Cu) presents a different surface structure. The Li_2O species is mostly absent and while there is a similar structure arising from reduced $(Tf)_2N^-$ species, progressing toward a LiF dominated SEI, there is also a significant quantity of hydrocarbon and C-N species not present on the native Li surface. These most likely arise from the $p^+_{1,X}$ cation, and are present as either reduced species or as cations physically entrained within the salt structure. The presence of Li_2O and Li_2CO_3 species is associated with a native film on the lithium surface.[4]

Diffuse reflectance FTIR (DRFTIR) spectroscopy.— Table I shows the Raman and IR spectrum peak positions and their assignments for $p_{1,X}(Tf)_2N$ electrolytes.

Figure 4 presents comparative spectra obtained from an uncycled $p_{1,4}(Tf)_2N$ electrolyte (transmission mode), the cycled Li surface, and the cycled Li-Cu surface. Significant differences can be observed that distinguish the spectra. The spectra obtained from the surface are dominated by that of the RTIL still present on the sample. As such, the differences could indicate changes that have occurred to the electrolyte itself, as well as the presence of surface species. Comparison of spectra of the electrolyte taken from cycled cells and of the uncycled electrolyte revealed that they were indistinguishable, indicating that the bulk electrolyte composition was unchanged with respect to its IR spectrum. Thus, the differences in appearance can be attributed to surface species and to differences in the spectral response of the two techniques. The two techniques should be comparable and peak positions should not change. However, changes in peak intensity are likely due to changes in the frequency response of the reflectivity of the sample surface. In addition, baseline correction will have introduced some differences in the intensity response, particularly at lower wavenumbers where the DRFTIR response was sloping.

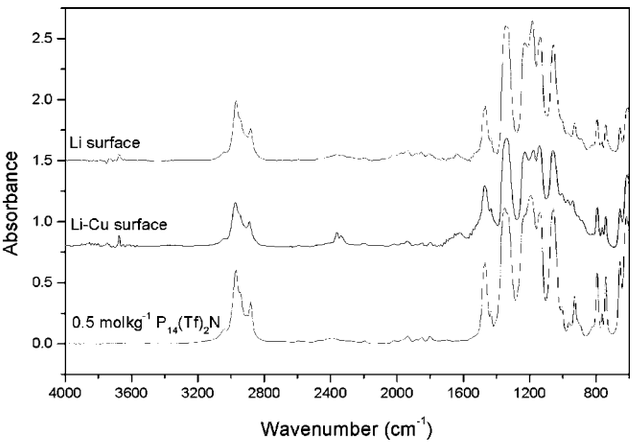

Figure 4. Comparative FTIR spectra for 0.5 mol kg^{-1} $Li(Tf)_2N$-$p_{1,4}(Tf)_2N$ electrolyte (transmission mode), the cycled Li surface, and the cycled Li-Cu surface.

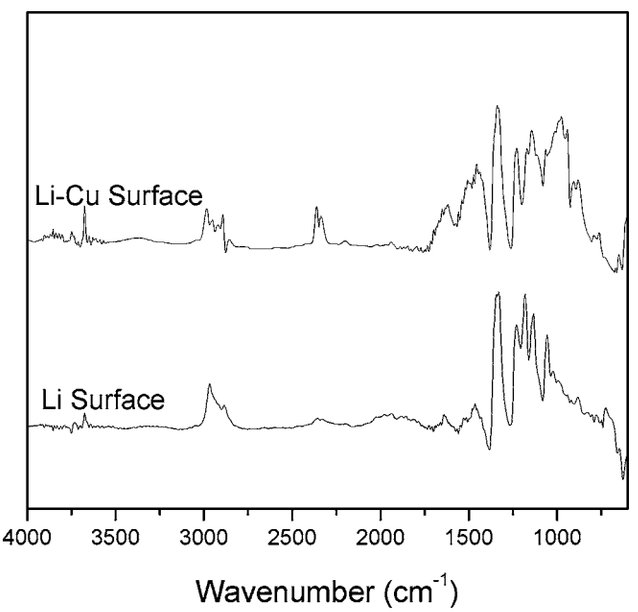

Figure 5. FTIR difference spectra obtained for the cycled Li-Cu surface, and the cycled Li surface.

Table II. Position and assignment for the most consistently prominent positive peaks in the difference spectrum for the Li-Cu surface cycled in a 0.5 mol kg^{-1} Li(Tf)$_2$N-p$_{1,X}$(Tf)$_2$N electrolyte.

Pos. peak (cm^{-1})	Assignment	Reference(s)
875	Li_2CO_3	33, 36, 43, and 44
905	Ring mode, C=C	41, 42, and 45
944	Ring mode, C=C	41, 42, and 45
977	Ring mode, C=C	41 and 42
1013	δSO_2	36, 37, and 46
1065	$\nu_a SNS$	36, 37, and 46
1145	$\nu_s SO_2$	36, 37, and 46
1171	$\nu_a CF_3$ (?)	36, 37, and 46
1229	$\nu_a CF_3$	36, 37, and 46
1338	$\nu_a SO_2$	36, 37, and 46
1440	Li_2CO_3	33, 43, and 44
1508	Li_2CO_3	33, 36, 43, and 44
1618	Amide, C=C	42
3675	LiOH	33, 43, and 47

Table IV. Position and assignment for the most consistently prominent positive peaks in the difference spectrum for the Li surface cycled in a 0.5 mol kg^{-1} Li(Tf)$_2$N-p$_{1,X}$(Tf)$_2$N electrolyte.

Pos. peak (cm^{-1})	Assignment	Reference(s)
879	Li_2CO_3	33, 36, 43, and 44
984		
1018	δSO_2	36, 37, and 46
1057	$\nu_s SO_2$	48
1110		
1136	$\nu_s SO_2$	36, 37, and 46
1184	$\nu_a CF_3$	36, 37, and 46
1332	$\nu_a SO_2$	36, 37, and 46
1345	$\nu_a SO_2$	36, 37, and 46
1530	Li_2CO_3	33, 36, 43, and 44
1642	Amide, C=C	42
2851	νCH_2	41
2919	νCH_2	41
2962	νCH_2	41
3676	LiOH	33, 43, and 47

The most informative way to compare spectra of this type is by subtraction, where a difference spectrum is obtained. In this case, the spectra were baseline corrected and normalized to the intensity of a single peak, and then the spectrum of the electrolyte was subtracted from the DRFTIR spectrum acquired from the surface. Interpretation of the difference spectrum is complicated by the comparison of the two different techniques and by the choice of the normalization peak. To avoid misinterpretation, a number of different peaks were used to normalize the spectra; the difference spectra acquired by normalizing to the peak at 794 cm^{-1} are shown in Fig. 5. Tables II and III provide tentative assignments for the peaks which consistently appeared in the Li-Cu difference spectrum, regardless of the choice of the normalization peak. Similarly, peak assignments are given for the Li difference spectrum in Tables IV and V.

Positive peaks most likely represent new species on the surface of the sample, either due to the formation of new bonds or due to the presence of larger amounts of materials with the same types of chemical bonds. The negative peaks most likely represent broken or missing/lost bonds and hence a loss in the intensity of a particular band, which indicate the species that have reacted to form the new surface compounds.

The peak assignments clearly indicate the presence of reduction products of the $(Tf)_2N^-$ anion on the surface of the Li-Cu electrode, providing strong support for the XPS results. The number of altered peaks indicates that the $(Tf)_2N^-$ anion had reacted in a complex manner. Considering the functional groups that could be reduced by lithium (e.g., $-CF_3$, $-SO_2$, S-N) the spectral evidence suggests that the anion had undergone reaction via a number of different pathways. The presence of Li_2CO_3 and LiOH is also indicated, again supporting the XPS interpretation. The presence of modes associated with the pyrrolidinium ring is also indicated, and the band at 1618 cm^{-1} suggests that the cation had also been reduced. The reduction could have occurred at the nitrogen, resulting in the formation of an amide, or possibly via the formation of a CF_3 radical which could extract an alkyl hydrogen, thus forming a C=C bond.[49] The evidence for the reduction of the cation is not clear and its presence could be due to physical entrainment within the SEI structure or by the precipitation of solid pyrrolidinium salts with reaction products of the $(Tf)_2N^-$ anion (e.g., pyrrolidinium triflate).

The difference spectrum obtained from the Li surface indicated the presence of reduction products of the $(Tf)_2N^-$ anion as well as LiOH and Li_2CO_3. The spectrum was also clearly different from that obtained from the Li-Cu surface, although it exhibited similar features. The pyrrolidinium cation appears to be less evident in this case.

It was noted when dismantling the cells that a significant amount of material would often adhere to the separator surface, particularly when a glass fibre filter paper was used as a separator. Figure 6 shows the difference spectrum obtained by subtracting the spectrum of the electrolyte from the spectrum obtained by wiping a NaCl IR plate with the Li facing surface of the separator, the difference spectra all exhibited the same features regardless of the normalization peak. The peak positions and assignments are summarized in Table VI. The difference spectrum indicates that the sample obtained from the surface of the separator was composed entirely of p$_{1,3}$(Tf)$_2$N electrolyte and reduction products of the $(Tf)_2N^-$ anion. This simple method is more robust because the difference spectrum is generated from two transmission spectra. Whether the sample obtained is representative of the entire SEI is debatable, however, taken with the results from the DRFTIR measurements, clear evidence for the reduction of the $(Tf)_2N^-$ anion is provided.

Raman spectroscopy.— The use of an optical cell allowed the acquisition of insitu Raman spectra. This enabled the electrolyte composition to be monitored as a function of cycling and allowed spectra to be obtained from the lithium surface.

Table III. Position and assignment for the most consistently prominent negative peaks in the difference spectrum for the Li-Cu surface cycled in a 0.5 mol kg^{-1} Li(Tf)$_2$N-p$_{1,X}$(Tf)$_2$N electrolyte.

Neg. Peak (cm^{-1})	Assignment	Reference(s)
1057	$\nu_s SO_2$	48
1202	$\nu_a CF_3$	36, 37, and 46
1253	$\nu_s CF_3$	36, 37, and 46
1372	Sulfonamide	42
2880	νCH_2	42

Table V. Position and assignment for the most consistently prominent negative peaks in the difference spectrum for the Li surface cycled in a 0.5 mol kg^{-1} Li(Tf)$_2$N-p$_{1,X}$(Tf)$_2$N electrolyte.

Neg. peak (cm^{-1})	Assignment	Reference(s)
1254	$\nu_s CF_3$	36, 37, and 46
1377	Sulfonamide	42

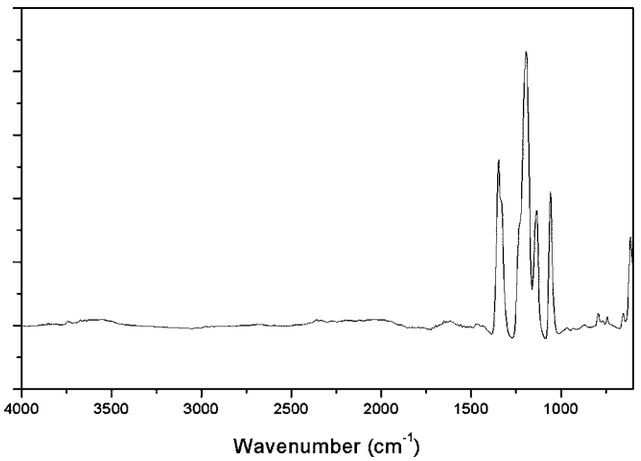

Figure 6. FTIR difference spectra obtained by sampling the surface of a separator taken from a cycled Li/0.5 mol kg^{-1} $Li(Tf)_2N$-$p_{1,3}(Tf)_2N$/Cu cell.

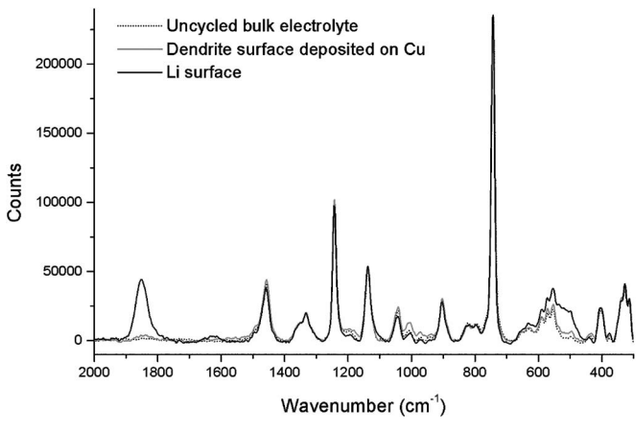

Figure 7. In situ Raman spectra acquired from a cycled optical cell containing 0.5 mol kg^{-1} $Li(Tf)_2N$-$p_{1,3}(Tf)_2N$ showing a comparison of the bulk electrolyte, the Li surface, and the Li surface deposited on a copper substrate (dendrite surface).

In situ Raman spectra acquired from 0.5 mol kg^{-1} $Li(Tf)_2N$-$p_{1,3}(Tf)_2N$ optical cells before and after cycling displayed no major discernible differences in the spectra indicating that significant chemical changes to the electrolyte composition had not occurred.

Figure 7 presents in situ Raman spectra acquired from a cycled 0.5 mol kg^{-1} $Li(Tf)_2N$-$p_{1,3}(Tf)_2N$ optical cell. Spectra were acquired from the cycled lithium surface (Li), a dendrite deposited on Cu (Li-Cu) and from the bulk electrolyte. The difference spectra for the Li surface and for the Li-Cu surface are shown in Fig. 8. The prominent peaks and their tentative assignments are given in Table VII and VIII respectively.

The Li surface difference spectrum exhibits some peaks that could be associated with $(Tf)_2N^-$ reduction products as well as a broad peak at 535 cm^{-1} that IR studies have reported to arise from Li_2O. The most prominent feature is the peak at 1853 cm^{-1}. Recently, a report in the literature dealt with the appearance of the peak at 1850 cm^{-1} in the Raman spectra obtained from lithium surfaces.[51] The authors demonstrated that the peak was associated with the thermal degradation of Li_2CO_3 (due to local heating of the Li surface by the laser). The peak was assigned to the stretching vibration of the C≡C bond; evidence was presented which indicated that the species formed was Li_2C_2. The Li-Cu difference spectrum is virtually featureless; the sharp peaks at 740 and 1243 cm^{-1} are likely to be due to band shifts in the peak position due to interactions with the lithium surface. The peak at 1849 cm^{-1} is very weak by comparison with that for the native lithium metal surface. This supports the assertion that the composition of the Li and Li-Cu surface films are significantly different, and that the differences arise from the presence of native film species persisting on the Li surface.

Electrochemical impedance spectroscopy (EIS): Fitting.— EIS has been shown to give an understanding of the nature of the SEI. However, the models used are often under debate. We have attempted to fit acquired impedance data with several models, the data for which is given in Table IX. The models used were the polymer electrolyte interphase (PEI) model, proposed by Thevenin and Muller,[52] and the layer model which was proposed and applied extensively by Aurbach et al.[53-55]

The majority of the error in the fits arose from contributions from fitting the high-frequency data. From this perspective, it is difficult to assert the superiority of one model over another and the development of a picture of the physical structure of the SEI from EIS alone is questionable. However, with the supporting information already provided, the EIS data can be incorporated to develop a model for the structure of the SEI. The best fits were obtained for the layer models, particularly the three- and four-element circuits employing constant phase elements. The addition of a fifth element to the layer model equivalent circuit did not show any improvement over the four-element circuit. The use of CPEs to describe the low frequency arc suggests a homogeneous dispersion of time constants,[56] indicating a complex composition where varied conduction pathways exist in parallel. The constant phase elements are used, in this case, to account for the departure from ideality of the capacitance behavior of the interface. This type of element is often used to describe real systems where the microscopic material properties are themselves distributed. For example, a solid electrode | solid electrolyte interface may have defects such as kinks, jags, ledges, local charge inhomogeneities, two and three-phase regions, adsorbed species, and variations in composition and stoichiometry.[56] The ability to fit the high frequency arc with a resistance/capacitance (RC) type circuit elements suggests a structure which has distinct elements (or layers), parallel to the electrode surface.[54] A layer model is attractive be-

Table VI. Position and assignments for peaks in the difference spectrum for a separator sample obtained from the separator of a cycled 0.5 mol kg^{-1} $Li(Tf)_2N$-$p_{1,x}(Tf)_2N$ cell.

Pos. peak (cm^{-1})	Assignment	Reference(s)
615	$\delta_a SO_2$	36, 37, and 46
1060	$\nu_s SO_2$	48
1135	$\nu_s SO_2$	36, 37, and 46
1193	$\nu_a CF_3$	36, 37, and 46
1234	$\nu_a CF_3$	36, 37, and 46
1331	$\nu_a SO_2$	36, 37, and 46
1349	$\nu_a SO_2$	36, 37, and 46

Table VII. Prominent peaks and tentative assignments for the Li surface Raman difference spectrum.

Pos. peak Li_2O	Assignment	Reference(s)
535	Li_2O (IR)	43 and 50
744	$\delta_s CF_3$	37, 39, and 40
787	$\tau CH_2, \nu_s CF_3$, C-S, S-O, etc.	36
1114		
1243	$\tau CH_2, \nu_s CF_3$	38
1614	Amide, C=C	42
1853	νC≡C	51
2059	Cyano (?)	36, 37, and 46

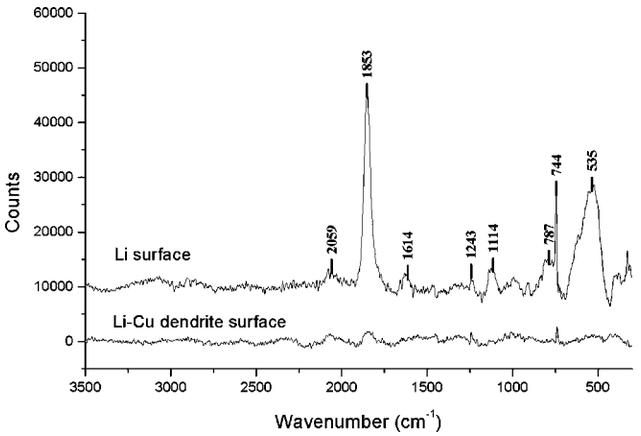

Figure 8. Raman difference spectra for the Li surface and the Li surface deposited on a copper substrate (dendrite surface) acquired from a cycled optical cell containing 0.5 mol kg^{-1} $Li(Tf)_2N$-$p_{1,3}(Tf)_2N$ electrolyte.

cause it agrees with evidence suggesting the formation of surface films comprised of inner compact and outer diffuse layers.[57]

The contribution from induction currents at high frequency prevents adequate modeling of the electrode response above 1 MHz. However, by using electrolyte conductivity values,[6] and accounting for the cell geometry and separator tortuosity it is possible to estimate the resistance contribution of the electrolyte (R_e). Values of approximately 4.5 Ω at 25°C are obtained, which is negligible compared to the resistance contribution of the high frequency arc (~225 Ω). Setting the value of R_c to 4.5 Ω resulted in the best fit being obtained by the four-element layer model, providing additional support for this model. An example of the fitted data is presented in Fig. 9. Further support is provided by the appearance of distinct activation energies for conduction within the SE1, presented in the next section.

Table VIII. Prominent peaks and tentative assignments for the Li-Cu surface Raman difference spectrum.

Pos. peak (cm^{-1})	Assignment	Reference(s)
740	$\delta_s CF_3$	37, 39, and 40
1243	$\tau CH_2, \nu_s CF_3$	38
1849	$\nu C{\equiv}C$	38
2075	Cyano (?)	36, 37, and 46

Considering the impedance plot in general terms, it is apparent that the bulk of the cell resistance arises from the process corresponding to the low-frequency arc (i.e., ~1425 Ω, Fig. 9). By comparison, the contribution for the high-frequency arc and the electrolyte resistance is trivial.

By using the capacitance values obtained for each arc, it is possible to estimate the thickness of each layer according to Eq. 5

$$l = \frac{\varepsilon_0 KA}{C} \qquad [5]$$

where ε_0 is the dielectric constant for vacuum, K is the films' dielectric constant, C is its capacitance, and A is the electrode geomet-

Table IX. Fitting models and fit parameters for a cycled $p_{1,X}(Tf)_2N$ symmetrical lithium cell.

Equivalent Circuit	X^2	Σ Squares
	0.0004	0.062
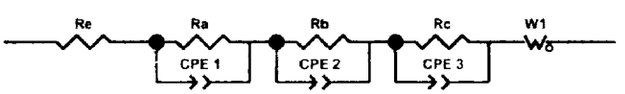	0.0002	0.034
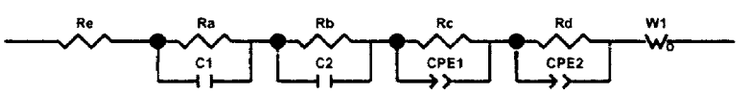	0.0002	0.024
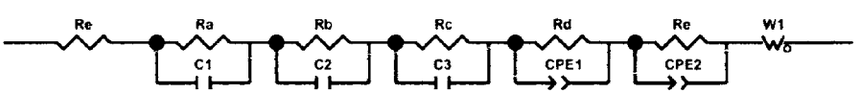	0.0002	0.024
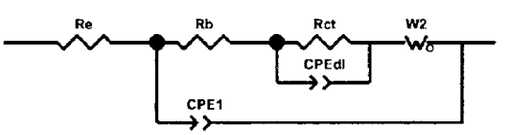	0.0022	0.307
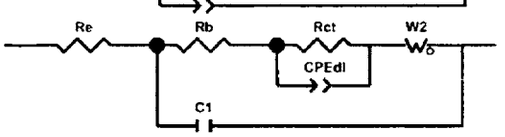	0.0004	0.048
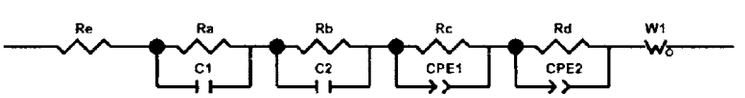 *	0.0006	0.084

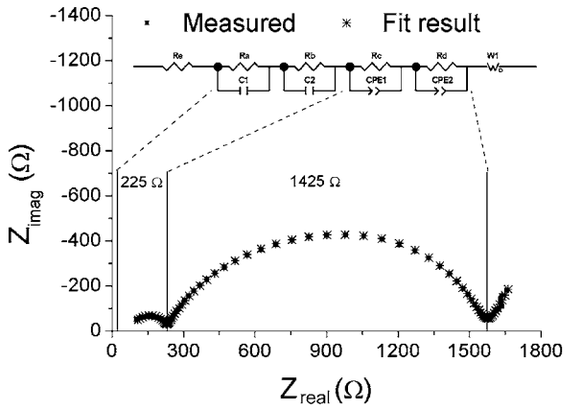

Figure 9. Example of a fitted impedance spectrum obtained from a cycled symmetrical lithium cell containing 0.5 mol kg^{-1} $Li(Tf)_2N$-$p_{1,3}(Tf)_2N$ electrolyte. The spectrum is fitted to a four-element layer model equivalent circuit; the error of the fit is shown.

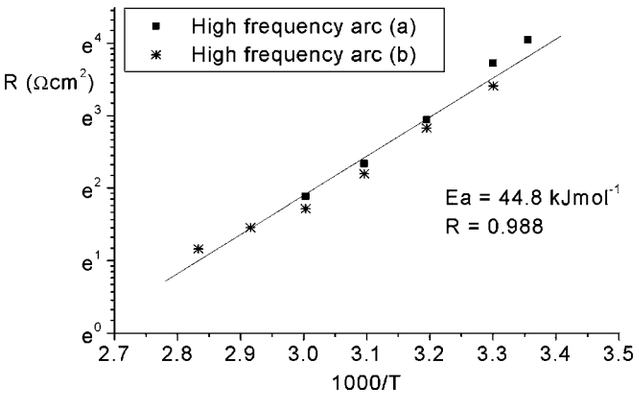

Figure 11. Arrhenius plot of the high-frequency arc resistance versus temperature for a cycled Li/0.5 mol kg^{-1} $Li(Tf)_2N$-$p_{1,3}(Tf)_2N$/Li cell: (a) temperature increasing, (b) temperature decreasing.

ric area.[55] The real capacitance (C_i) for a CPE can be calculated from Eq. 6[58]

$$C_i = R_i^{(1-n)/n} Y_i^{1/n} \quad [6]$$

where R_i is the resistance described by the arc and Y_i is a pseudocapacitance. The calculated capacitance for the high-frequency arc was of the order of 5×10^{-8} F, and the low-frequency arc was 5×10^{-7} F. Assuming a value of 5 for K for the high-frequency arc (based on Li_2O, LiF, etc.)[54] and a value of 10 for K for the low-frequency arc (based on ε ranging from 5 to 20 for most materials)[58] and a geometric area of 2 cm^2 for the electrode area, the film thickness can be estimated. These capacitance values reflect a layer ~180 nm thick for the high-frequency arc and ~40 nm thick for the low-frequency arc. Calculated resistivity values of 2.6×10^7 Ω cm and 7.4×10^8 Ω cm (both at 25°C), for the low- and high-frequency arcs, respectively, are comparable to those obtained for compact surface films formed in alkyl carbonates and ethers.[55]

Electrochemical impedance spectroscopy (EIS): Effects of temperature.— A structure composed of discrete layers, which are related to time constants represented by the elements of the equivalent circuit, should show varied response to temperature changes according to the physical properties of the individual layers. Measuring the impedance response of a cell at varied temperatures allows Arrhenius plots of resistance versus temperature to be constructed and, hence, determination of activation energies for each of the time constants corresponding to the high-frequency and low-frequency arcs in the Nyquist plot.

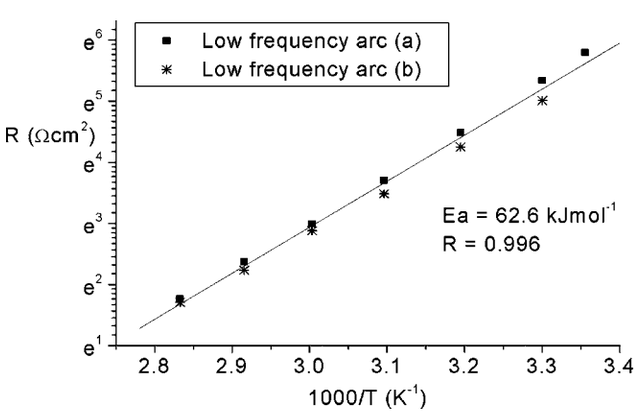

Figure 10. Arrhenius plot of the low-frequency arc resistance versus temperature for a cycled LI/0.5 mol kg^{-1} $Li(Tf)_2N$-$p_{1,3}(Tf)_2N$/Li cell: (a) temperature increasing, (b) temperature decreasing.

Figures 10 and 11 present Arrhenius plots obtained from a cycled 0.5 mol $kg^{-1}$$Li(Tf)_2N$-$p_{1,3}(Tf)_2N$ cell for the low-frequency and high-frequency arcs respectively. The plots indicate that Li^+ transport through the surface film occurs by at least two distinct conduction mechanisms, reflected by activation-energies for conduction of 45 and 60 kJ mol^{-1} for the high- and low-frequency arcs, respectively. These values are comparable to those obtained by similar methods for alkyl carbonate and ether based solvent systems.[53]

The presence of distinct conduction mechanisms has been rationalised by Aurbach et al.[53-55] in terms of the layer model, which was applied extensively to alkyl carbonate and ether electrolytes with varying lithium salts. The SE1 was viewed as a multi-layer structure, comprised of an inner compact interphase and an outer diffuse interphase. The compact interphase was composed of several distinct layers, each of which was found to exhibit distinct physicochemical properties. The inner layers of the compact interphase, which corresponded to the high-frequency part of the Nyquist plot, were found to be thickest, to have the lowest resistivity and to exhibit a low activation energy for conduction. Layers further from the lithium surface, closer to the solution side, were thinner, more resistive and had higher activation energies for conduction. The properties of the layers were discussed in terms of their proximity to the reactive lithium surface; the inner layers formed rapidly under less selective conditions and were expected to be composed of species with less complex chemical structures (i.e., Li_2O, LiF, etc.). These conditions produce a layer that is expected to be the most conductive because it has the greatest amount of defects present in its structure (due to the less selective formation conditions). By the same reasoning, the activation energy for conduction is also expected to be low. The factors that facilitate Li^+ migration through the film (e.g., defects) are also expected to facilitate electron transfer,[54] thus the layer which is the most disordered should also be the thickest. The outer layers form under more selective conditions, because of the presence of the insulating inner layer, and are expected to be composed of species with more complex chemical structures. The outer layers are expected to be more homogeneous, and are also expected to exhibit higher activation energies.[53,54]

All of the above observations agree well with the results presented here for the lithium surface in the RTIL. The calculated film thickness in the RTIL appears to be greater than those reported for alkyl carbonates, which range from 10-100 nm.[5] The other distinct difference between the data presented here seems to be the absence of the porous outer layer, which has been characterized by high capacitance (as a result of its high surface area), high resistivity

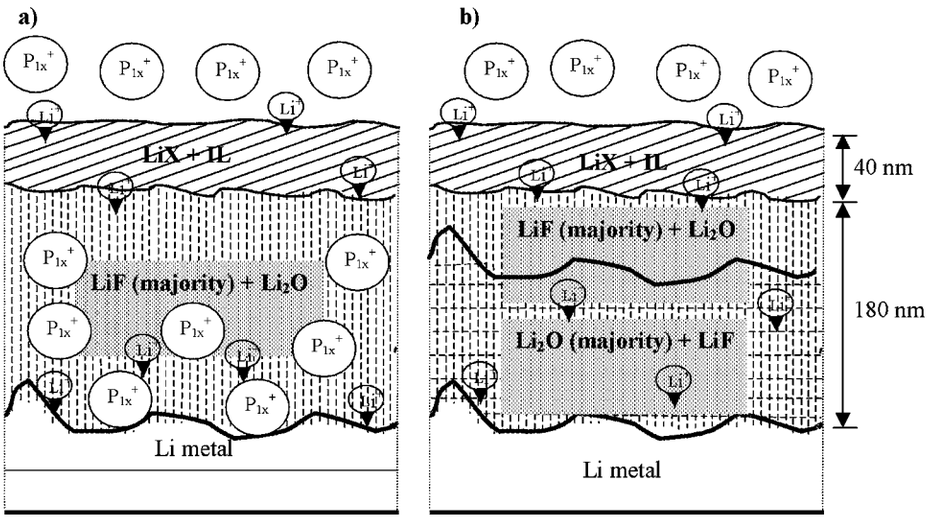

Figure 12. Simple models of the SEI structure on the Li (a) and the Li-Cu (b) surfaces. Li*X*:*X* can be S_2O_4, F, SO_3CF_3, NSO_2CF_3, SO_3, CO_3, S, O, or OH.

($>10^{10}$ Ω cm) and low activation energy. The outer layer in the RTIL (corresponding to the low frequency arc), while being highly resistive, exhibits high activation energy.

Li surface vs Li-Cu surface.— The difference in the composition of the films (Li and Li-Cu) can be rationalised by considering the conditions under which they were formed:

1. The Li surface was usually allowed to equilibrate for 24 h prior to cycling. Under these conditions, it appears that the passivating film already present on the lithium prevented any reduction/incorporation of the cation. The cation is unlikely to react, being stable at the lithium potential. Instead the $(Tf)_2N^-$ anion reacted, forming a protective film composed entirely of native film plus anion reduction products.

2. The Li-Cu surface was formed under more extreme conditions, the potential being at the lithium potential plus the overpotential necessary to maintain the current density. Under these conditions, reduction of the $p^+_{1,X}$ cation is possible. The $(Tf)_2N^-$ anion will definitely be reduced, commencing at approximately +1.5 V vs Li/Li^+.[55] In addition, the concentration of $p^+_{1,X}$ at the electrode surface will be high, because of electrostatic attraction. Thus, the formation of a film comprised of $(Tf)_2N^-$ reduction products with either reduced or entrapped $p^+_{1,X}$ species is more likely on the copper surface. The rate of lithium deposition is likely to have a pronounced effect on the composition and structure of the film.

A generalized model can be constructed for the structure of the SEI formed on the Li and Li-Cu surface; as shown in Fig. 12. The complimentary techniques used to obtain a detailed picture of the SEI were highly consistent. The simplified models shown in Fig. 12 highlight the principal differences between the Li and Li-Cu SEIs. The models indicate a layered structure, based on XPS and EIS evidence, and the approximate relative thickness of each layer is shown. The presence of significant quantities of Li_2O on the Li surface is indicated, as opposed to a LiF dominated inner layer on the Li-Cu surface. The presence of species related to $p^+_{1,X}$ is also indicated for the Li-Cu surface.

Conclusions

The SEI formed on the lithium electrode in a $p_{1,X}(Tf)_2N$ electrolyte was characterized using XPS, FTIR, Raman, and EIS techniques. This multipronged approach has allowed us to develop an understanding of the composition and structure of the SEI. XPS, FTIR, and Raman spectroscopy indicated that the SEI was mainly composed of reduction products of the anion.

A pronounced difference in composition was observed between the SEI formed on the lithium surface and that formed in situ during deposition. This had been expected from differences observed in the cycling properties and deposit morphologies exhibited in optical cells.[6] The native species present on the lithium surface appeared to persist in the SEI and to dominate the SEI composition. The surface film formed on the lithium deposit did not contain species associated with the lithium native film. Instead, significant quantities of species associated with the cation were observed. The role of the cation in the formation of the SEI is not clear at this stage. Some evidence of reduced species of the cation was indicated by the FTIR measurements, but the results were not conclusive.

The cation could be present in the surface film, trapped within the crystal structure of the anion reduction products. Alternatively, the cation could precipitate as solid $p_{1,X}$ salts of the reduction products of the anion (e.g., $p_{1,X}SO_2CF_3$). Kariv-Miller et al.[59,60] studied the reduction of quaternary ammonium cations on the surface of metals and reported the formation of metastable metal amalgams (Sn, Bi, Pb, Hg, and Sb). The formation of amalgams was typically electrochemically reversible. The formation of a $p_{1,X}(Li)_y$ amalgam should also be considered.

EIS indicated varied lithium conduction pathways through the film. Equivalent circuit modeling indicated that the pathways were in series and suggested a layered structure. Calculated activation energies, resistivity, and thickness values were comparable to literature values and indicated that the layered structure became progressively more conductive (i.e., more disordered) close to the lithium surface.

The work detailed here represents the first report in the literature of the characteristics of the lithium SEI formed in RTIL electrolytes. The importance of the finding that composition of the SEI is comprised of products of one of the ions (in this case the anion) should not be underestimated. In this respect, the RTILs offer an electrolyte system that has the potential to allow researchers a degree of control over the SEI composition that has not previously existed.

Acknowledgment

Funding from the ARC Centre for Nanostructured Electromaterials is gratefully acknowledged.

References

1. I. Yoshimatsu, T. Hirai, and J. Yamaki, *J. Electrochem. Soc.*, **135**, 2422 (1988).
2. E. Peled, *J. Electrochem. Soc.*, **126**, 2047 (1979).
3. E. Peled, D. Golodnitsky, and G. Ardel, *J. Electrochem. Soc.*, **144**, L208 (1997).
4. J.-I. Yamaki and S.-I. Tobishima, *Handbook of Battery Materials*, J. O. Besenhard, Editor, p. 339, Wiley-VCH, Weinheim, Germany (1999).
5. E. Peled, D. Golodnitsky, and J. Penciner, *Handbook of Battery Materials*. J. O. Besenhard, Editor, p. 419, Wiley-VCH, Weinheim, Germany (1999).
6. P. C. Howlett, D. R. MacFarlane, and A. F. Hollenkamp, *Electrochem. Solid-State Lett.*, **7**, A97 (2004).

7. V. R. Koch, C. Nanjundiah, G. B. Appetecchi, and B. Scrosati, *J. Electrochem. Soc.*, **142**, L116 (1995).
8. R. T. Carlin and J. Fuller, U.S. Pat. 5,589,291-A (1996).
9. J. Caja, T. D. J. Dunstan, V. Katovic, and D. M. Ryan, in *Proceedings of the 39th Power Sources Conference*, p. 124 (2000).
10. H. Matsumoto, H. Kageyama, and Y. Miyazaki, *Electrochemistry (Tokyo, Jpn.)*, **71**, 1058 (2003).
11. T. E. Sutto, P. C. Trulove, and H. C. De Long, *Electrochem. Solid-State Lett.*, **6**, A50 (2003).
12. Y. Katayama, M. Yukumoto, and T. Miura, *Electrochem. Solid-State Lett.*, **6**, A96 (2003).
13. M. Holzapfel, A. Martinent, F. Alloin, B. Le Gorrec, R. Yazami, and C. Montella, *J. Electroanal. Chem.*, **546**, 41 (2003).
14. M. Holzapfel, C. Jost, and P. Novák, *Chem. Commun. (Cambridge)*, **2004**, 2098 (2004).
15. T. Sato, T. Maruo, S. Marukane, and K. Takagi, *J. Power Sources*, **138**, 253 (2004).
16. M. Holzapfel, C. Jost, A. Prodi-Schwab, F. Krumeich, A. Würsig, H. Buqa and P. Novák, *Carbon*, **43**, 1488 (2005).
17. H. Matsumoto and Y. Miyazaki, *Yoyuen Oyobi Koon Kagaku*, **44**, 7 (2001).
18. J.-H. Shin, W. A. Henderson, and S. Passerini, *Electrochem. Commun.*, **5**, 1016 (2003).
19. H. Sakaebe and H. Matsumoto, *Electrochem. Commun.*, **5**, 594 (2003).
20. B. Garcia and M. Armand, *J. Power Sources*, **132**, 206 (2004).
21. J. H. Shin, W. A. Henderson, and S. Passerini, *Electrochem. Solid-State Lett.*, **8**, A125 (2005).
22. J. H. Shin, W. A. Henderson, G. B. Appetecchi, F. Alessandrini, and S. Passerini, *Electrochim. Acta*, **50**, 3859 (2005).
23. J. H. Shin, W. A. Henderson, and S. Passerini, *J. Electrochem. Soc.*, **152**, A978 (2005).
24. Y. Katayama, T. Morita, M. Yamagata, and T. Miura, *Electrochemistry (Tokyo, Jpn.)*, **71**, 1033 (2003).
25. D. R. MacFarlane, P. Meakin, J. Sun, N. Amini, and M. Forsyth, *J. Phys. Chem. B*, **103**, 4164 (1999).
26. P. C. Howlett, D. R. MacFarlane, and A. F. Hollenkamp, *J. Power Sources*, **114**, 277 (2003).
27. J. F. Moulder, W. F. Stickle, P. E. Sobol, and K. D. Bomben, *Handbook of X-Ray Photoelectron Spectroscopy*, Perkin-Elmer Corporation, Eden Prairie, MN (1992).
28. D. Aurbach, M. Daroux, P. Faguy, and E. Yeager, *J. Electroanal. Chem. Interfacial Electrochem.*, **297**, 225 (1991).
29. L. J. Rendek, G. S. Chottiner, and D. A. Scherson, *J. Electrochem. Soc.*, **149**, E408 (2002).
30. K. Kanamura, S. Shiraishi, H. Tamura, and Z. Takehara, *J. Electrochem. Soc.*, **141**, 2379 (1994).
31. I. Ismail, A. Noda, A. Nishimoto, and M. Watanabe, *Electrochim. Acta*, **46**, 1595 (2001).
32. K. Kanamura, H. Tamura, S. Shiraishi, and Z.-I. Takehara, *Electrochim. Acta*, **40**, 913 (1995).
33. K. Morigaki and A. Ohta, *J. Power Sources*, **76**, 159 (1998).
34. K. Kanamura, H. Tamura and Z. Takehara, *J. Electroanal. Chem.*, **333**, 127 (1992).
35. H. Ota, Y. Sakata, X. Wang, J. Sasahara and E. Yasukawa, *J. Electrochem. Soc.*, **151**, p-A446 (2004).
36. D. Aurbach, I. Weissman, A. Zaban and O. Chusid, *Electrochim. Acta*, **39**, 51 (1994).
37. I. Rey, P. Johansson, J. Lindgren, J. C. Lassègues, J. Grondin and L. Servant, *J. Phys. Chem. A*, **102**, 3249 (1998).
38. J. Adebahr, P. Johansson, P. Jacobsson, D. R. MacFarlane and M. Forsyth, *Electrochim. Acta*, **48**, 2283 (2003).
39. I. Rey, J. L. Bruneel, J. Grondin, L. Servant and J. C. Lassegues, *J. Electrochem. Soc.*, **145**, 3034 (1998).
40. Z. Wang, W. Gao, X. Huang, Y. Mo and L. Chen, *J. Raman Spectrosc.*, **32**, 900 (2001).
41. B. Bednarska-Bolek, R. Jakubas, G. Bator and J. Baran, *J. Mol. Struct.*, **614**, 151 (2002).
42. D. H. Williams and I. Fleming, *Spectrocopic Methods in Organic Chemistry*, McGraw-Hill Book Company (UK) Limited, Maidenhead (1980).
43. D. Aurbach, *J. Electrochem. Soc.*, **136**, 1611 (1989).
44. J. Li, H. Li, Z. Wang, L. Chen and X. Huang, *J. Power Sources*, **107**, 1 (2002).
45. C. N. R. Rao, *Chemical Applications of Infrared Spectroscopy*, Academic Press, New York (1963).
46. O. Chusid, Y. Gofer, D. Aurbach, M. Watanabe, T. Momma, and T. Osaka, *J. Power Sources*, **97-98**, 632 (2001).
47. K. Nakamoto, *Infrared Spectra of Inorganic and Coordination Compounds*, Wiley-Interscience, New York (1970).
48. H. Every, A. G. Bishop, M. Forsyth, and D. R. MacFarlane, *Electrochim. Acta*, **45**, 1279 (2000).
49. M. Le Granvalet-Mancini, T. Hanrath, and D. Teeters, *Solid State Ionics*, **135**, 283 (2000).
50. D. Aurbach, M. L. Daroux, P. W. Faguy, and E. Yeager, *J. Electrochem. Soc.*, **134**, 1611 (1987).
51. C. Naudin, J. L. Bruneel, M. Chami, B. Desbat, J. Grondin, J. C. Lassc̆gues, and L. Servant, *J. Power Sources*, **124**, 518 (2003).
52. J. G. Thevenin and R. H. Muller, *J. Electrochem. Soc.*, **134**, 273 (1987).
53. A. Zaban, E. Zinigrad, and D. Aurbach, *J. Phys. Chem.*, **100**, 3089 (1996).
54. D. Aurbach and A. Zaban, *J. Electroanal. Chem.*, **367**, 15 (1994).
55. *Nonaqueous Electrochemistry*, D. Aurbach, Editor, Marcel Dekker, New York (1999).
56. J. Ross Macdonald, *Impedance Spectroscopy: Emphasizing Solid Materials and Systems.*, Wiley-Interscience, New York (1987).
57. Y. Geronov, F. Schwager, and R. H. Muller, *J. Electrochem. Soc.*, **129**, 1422 (1982).
58. R. Bouchet, S. Lascaud, and M. Rosso, *J. Electrochem. Soc.*, **150**, A1385 (2003).
59. E. Kariv-Miller, P. B. Lawin, and Z. Vajtner, *J. Electroanal. Chem. Interfacial Electrochem.*, **195**, 435 (1985).
60. C. M. Ryan, V. Svetlicic, and E. Kariv-Miller, *J. Electroanal. Chem. Interfacial Electrochem.*, **219**, 247 (1987).